

Physics-informed neural networks for viscoacoustic wave propagation: forward modelling, inversion and discretization sensitivity

Chaohua Liang¹, Xingliang Peng², Jun Matsushima^{1*}

¹ The University of Tokyo
Graduate School of Frontier Sciences
Kashiwa, Japan

² College of Water Conservancy, Jiangxi University of Water Resources and Electric Power
Nanchang 330099, China

SUMMARY

Seismic wave forward and inverse modeling not only provide the theoretical foundation for understanding the Earth's complex deep structures, but also constitute core techniques for subsurface resource exploration and geological hazard assessment. Traditional numerical approaches, such as the finite-difference method (FDM) and finite-element method (FEM), typically rely on grid-based discretization and iterative forward simulations when solving inverse problems. Although deep learning has shown considerable potential in seismic applications, its effectiveness is often limited by the requirement for large volumes of labelled data and the insufficient incorporation of physical constraints. In this study, we propose a unified physics-informed neural network (PINN) framework for both forward modeling and parameter inversion of viscoacoustic wave propagation. The proposed framework is validated through comparative numerical experiments. For forward modeling, the network accurately reproduces wavefields, amplitude attenuation, and phase characteristics across different velocity models. For inversion, we evaluate the reconstruction of velocity and attenuation models from temporally sparse observations and random initial guesses. The results indicate that the proposed PINN approach achieves stable and acceptable accuracy when benchmarked against reference solutions, while exhibiting reduced sensitivity to spatial discretization compared with grid-based numerical methods. More importantly, by embedding a viscoacoustic wave equation into the learning process, the framework provides a physically consistent representation of intrinsic attenuation effects beyond purely acoustic approximations. In addition, the capability of simultaneously recovering velocity and attenuation parameters under sparse sampling conditions highlights the robustness and flexibility of the proposed method. These results demonstrate the feasibility of the method and highlight its potential for high-resolution seismic exploration.

Key words: Physics-Informed Neural Networks (PINNs), Viscoacoustic wave, Forward and inverse modeling, Attenuation and dispersion, Seismic exploration.

1 INTRODUCTION

Accurate seismic imaging is essential for resolving subsurface geological structures, particularly in the exploration and assessment of energy resources such as methane hydrates, commonly referred to as “combustible ice” owing to their high energy density and widespread occurrence. Over the past few decades, numerical methods such as the finite difference method (FDM) and finite element method (FEM) have been firmly established as the standard tools for seismic forward modeling and inverse analysis (Liu & Sen(2011); Nogueira & Porsani(2021); Pled & Descliers(2022)).

These grid-based approaches typically discretize the domain into meshes to approximate the partial differential equations (PDEs). Although conventional approaches, such as FDM and full waveform inversion (FWI), can achieve high accuracy in solving partial differential equations, they rely on repeated high-fidelity forward simulations during inversion, which leads to substantial computational cost. What's more, the misfit function of FWI is prone to converging toward local minima rather than the global optimum (Virieux & Operto(2009)).

With the rapid evolution of deep learning (DL), together with the exponential increase in GPU-accelerated computing power, data-driven paradigms have witnessed explosive growth in the field of seismology. The enhanced hardware capabilities have allowed

* Corresponding author: jun-matsushima@edu.k.u-tokyo.ac.jp

researchers to train sophisticated neural networks on massive seismic datasets, establishing complex non-linear mappings between measurements and subsurface properties. For example, Wu and Lin (Wu & Lin(2020)) proposed InversionNet, a framework that employs a deep convolutional encoder-decoder architecture to directly learn the non-linear mapping from seismic data to subsurface velocity structures. Similarly, Recurrent Neural Networks (RNNs) have been successfully applied to seismic impedance inversion (Alfarraj & AlRegib(2019)), leveraging the temporal correlations within seismic traces. Furthermore, Generative Adversarial Networks (GANs) have shown remarkable performance in seismic data reconstruction (Li et al.(2025) Li, Liu, & Zu). However, these supervised methods require lots of labeled data, which is difficult to obtain in real-world seismic exploration. Besides, these models are essentially black-box mappers, therefore may generate physically unreasonable results.

Recently, Physics-informed neural networks (PINNs) by Raissi (Raissi et al.(2019) Raissi, Perdikaris, & Karniadakis) have received widespread attention as a new scientific computation algorithm. PINNs explicitly embed the governing Partial Differential Equations (PDEs) into the loss function as a regularization mechanism, which provides new ideas for addressing problems faced in conventional methods. Specifically, in inverse problems, PINNs integrate the forward and inverse processes into a unified framework. By treating the unknown parameters in PDEs as trainable variables, PINNs leverage automatic differentiation to update these parameters simultaneously with the outputs of the forward process. PINNs are now applied to miscellaneous scientific domains including fluid mechanics (Raissi et al.(2019) Raissi, Perdikaris, & Karniadakis; Raissi et al.(2020) Raissi, Yazdani, & Karniadakis), geophysics (Rasht-Behesht et al.(2021) Rasht-Behesht, Huber, Shukla, & Karniadakis; Ren et al.(2022) Ren, Rao, Chen, Wang, Sun, & Liu), solid mechanics (Haghigat et al.(2021) Haghigat, Raissi, Moure, Gomez, & Juanes), heat transfer (Zhao et al.(2025) Zhao, Wang, Zhang, Ba, & Sun) and biomedical imaging (Wong et al.(2025) Wong, Chan, Mao, & Yap).

However, vanilla PINNs face certain challenges in seismic exploration. Studies indicate that vanilla PINNs suffer from point-source singularity in solving wave equations. To address this problem, a hybrid initialization strategy that utilizes the solutions generated by the FDM method at early time steps as initial constraints is proposed (Alkhalifah et al.(2021) Alkhalifah, Song, Waheed, & Hao). What's more, while Physics-Informed Neural Networks (PINNs) have recently emerged as a powerful tool for solving seismic wave equations, the majority of existing studies restrict their scope to ideal acoustic or elastic media (Rasht-Behesht et al.(2021) Rasht-Behesht, Huber, Shukla, & Karniadakis; Ren et al.(2022) Ren, Rao, Chen, Wang, Sun, & Liu; Zou et al.(2024) Zou, Liu, Zhao, & Song), explicitly neglecting the intrinsic attenuation properties of the subsurface. However, in realistic geological formations, the viscosity of rocks and the presence of fluids inevitably cause the conversion of mechanical energy into heat. This phenomenon, known as seismic absorption, induces velocity dispersion and amplitude dissipation, which significantly alter the waveform characteristics (Malinowski et al.(2011) Malinowski, Operto, & Ribodetti). Furthermore, their application to inverse problems—particularly in complex viscoacoustic media—remains noticeably underexplored. To address these limitations, we establish a physics-informed architecture specifically designed to capture these complex viscoacoustic behaviors and is able to run forward and inverse process simultaneously.

In this paper, we propose a unified physics-informed neural network framework for viscoacoustic wave propagation, capable of both forward modeling and physical parameter inversion. To avoid point-source singularities, early-time wavefields are incorporated as initial constraints, and open boundary conditions are employed to suppress artificial boundary reflections. The main contributions of this work are threefold. First, we demonstrate that the proposed framework accurately models viscoacoustic wavefields, capturing both attenuation and phase characteristics in homogeneous and layered velocity models. Second, we show that the PINN formulation remains stable under coarse discretization and sparse sampling conditions, exhibiting a fundamentally different degradation behavior compared to finite-difference solvers. Third, we introduce a simultaneous forward-inverse strategy that enables robust recovery of both velocity and absorption parameters from random initial models, highlighting the framework's ability to solve the inverse problem by treating physical parameters as learnable variables.

2 PROBLEM FORMULATION

In this paper, our goal is to investigate the ability of PINNs for viscoacoustic propagation in 2D homogeneous media. The governing equations based on the Maxwell rheological model for propagating pressure in the time-space domain are given by (Deng & McMechan(2007)):

$$\frac{1}{v^2} \frac{\partial^2 P}{\partial t^2} - \nabla^2 P + \frac{g}{v} \frac{\partial P}{\partial t} = S(x_s, t) \quad (1)$$

Where P , v , and t denote the pressure, velocity, and time, respectively. S represents the source term. Consistent with standard seismic modeling practices, a Ricker wavelet is employed as the source function in this study. g is the absorption coefficient, given by:

$$g = \frac{2\pi f_0}{vQ} \quad (2)$$

Where f_0 and Q denote the reference frequency and the quality factor, respectively. The quality factor Q is analytically derived from Li's empirical formula:

$$Q = 3.516 \times 10^{-6} \times v^{2.2} \quad (3)$$

It is noteworthy that the governing equation employed in this study, derived from the equations proposed by (Deng & McMechan(2007)), represents a pragmatic numerical approximation of wave propagation in viscoacoustic media. It is essential to acknowledge that this model assumes a frequency-independent velocity v and quality factor Q within a limited bandwidth. While this approximation neglects the subtle effects of frequency-dependent dispersion, it is a suitable tradeoff for PINNs training, as it provides a stable and differentiable residual for the loss function while maintaining sufficient accuracy for most exploration-scale applications.

In this study, the objective is to perform forward and inverse simulations for viscoacoustic wave propagation using physics-informed neural networks (PINNs). More specifically, in forward modeling, we solve the viscoacoustic wave equation by relying only on time-sparse data and physical laws, including the governing partial differential equations (PDEs) and boundary conditions. In the inversion scheme, PINNs are utilized to simultaneously reconstruct the wavefield and invert for the velocity and absorption coefficient from sparse time-domain measurements.

3 METHODOLOGY

In this section, we proposed a PINN architecture for both forward and inverse problems. In forward problems, a fully connected network is applied, while in inversion, we utilize a Fourier feature neural network to represent the wavefield P to mitigate the gradient vanishing problems, which lead to divergence of the network. Furthermore, considering the characteristics of seismic exploration, we apply open boundary conditions on the boundaries of the domain to eliminate the reflection. In addition, wavefields at early timesteps by FDM are utilized as initial constraints to overcome the point-source singularity.

3.1 PINNs

Deep learning (DL) has garnered significant interest in seismic exploration. However, conventional DL approaches for seismic analysis typically require massive volumes of labeled training data, which are often expensive or impossible to acquire in real-world exploration. Recently, Physics-Informed Neural Networks (PINNs) have received great attention because of their ability of learning in data-scarce regimes by encoding physical laws (i.e., governing PDEs and boundary conditions) into the network constraints.

Structurally, a physics-informed neural network (PINN) is similar to a conventional multilayer perceptron (MLP). It is composed of an input layer, several fully connected hidden layers, and an output layer. Let N_L denote the total number of layers. The mapping from the $(l-1)$ -th layer to the l -th layer can be mathematically formulated as

$$\mathbf{h}^{(l)} = \sigma \left(\mathbf{W}^{(l)} \mathbf{h}^{(l-1)} + \mathbf{b}^{(l)} \right), \quad l = 1, \dots, N_L, \quad (4)$$

where $\mathbf{W}^{(l)}$ and $\mathbf{b}^{(l)}$ represent the weight matrix and bias vector of the l -th layer, respectively, and σ denotes a nonlinear activation function (e.g., \tanh or SiLU).

The main difference between PINNs and conventional MLPs lies in the loss function. In PINNs, the loss function explicitly incorporates the governing equations as physical constraints. By minimizing this physics-informed loss function, PINNs are able to approximate solutions to partial differential equations (PDEs). For inverse problems, PINNs treat unknown physical parameters (e.g., velocity and quality factor) as trainable variables. These parameters are optimized simultaneously with the neural network weights by minimizing a composite loss function.

3.2 Open Boundary Conditions

In conventional grid-based methods, such as finite difference methods (FDM), Perfect Matched Layers (PML) are typically employed to eliminate boundary reflections by artificially damping waves in an extended domain. However, implementing PML requires additional auxiliary equations, which significantly complicates the loss landscape when incorporated into the optimization objective. Furthermore, PML requires the construction of extended sponge layers, inevitably leading to a larger number of collocation points and increased computational cost. Consequently, employing PML is considered computationally inefficient for the proposed PINN framework. Instead, we apply a first-order open boundary condition directly at the domain edges, which effectively allows waves to exit the computational domain without reflection.

Specifically, the formulas of first-order open boundary condi-

tions are given by:

$$\frac{\partial P}{\partial t} - v \frac{\partial P}{\partial x} = 0, \quad \text{at } x = 0 \quad (5)$$

$$\frac{\partial P}{\partial t} + v \frac{\partial P}{\partial x} = 0, \quad \text{at } x = L \quad (6)$$

$$\frac{\partial P}{\partial t} - v \frac{\partial P}{\partial y} = 0, \quad \text{at } y = 0 \quad (7)$$

$$\frac{\partial P}{\partial t} + v \frac{\partial P}{\partial y} = 0, \quad \text{at } y = L \quad (8)$$

Here, $\{x, y, t\}$ denote the spatial and temporal coordinates, respectively. P represents the pressure wavefield, $dLen$ is the domain length, and v is the propagation velocity. Physically, these conditions enforce one-way wave propagation behavior at the truncation edges ($x = 0, x = L, y = 0, y = L$), ensuring that seismic energy radiates out of the computational domain without generating reflections.

3.3 Network architecture

Firstly, to clarify, in order to overcome the numerical challenges posed by point-source singularities during the PINN training process, the external source term S is removed from the governing equation. Instead, the initial state of the system is constrained using early-time wavefields generated by the finite-difference method (FDM), which will be discussed later. Moreover, Eq. (1) is reformulated by multiplying both sides by v^2 to avoid potential numerical issues associated with the $1/v^2$ term. Consequently, the governing equation employed in the proposed framework can be expressed as:

$$\frac{\partial^2 P}{\partial t^2} - v^2 \nabla^2 P + gv \frac{\partial P}{\partial t} = 0 \quad (9)$$

In the following sections, we let g denote the product of gv to simplify the notation of the loss function.

The overall architecture of the proposed PINN framework is illustrated in Fig. 1. To accommodate both forward and inverse modeling tasks, the framework adopts a modular design consisting of three distinct neural networks that approximate the pressure field P (P-Net), the velocity field v (v-Net), and the absorption coefficient g (g-Net), respectively.

For forward problems, the objective is to simulate wave propagation in a known medium. Therefore, the propagation velocity v and absorption coefficient g are fixed, implying that the v-Net and g-Net are deactivated. The network takes the mapped features $\{x, y, t\}$ as inputs and outputs the pressure field P . After obtaining P , the required partial derivatives with respect to the input coordinates $\{x, y, t\}$ are computed via automatic differentiation.

For inverse problems, the goal is to simultaneously reconstruct the wavefield and the unknown medium parameters from sparse observational data. In this case, the propagation velocity v and absorption coefficient g are treated as learnable, spatially dependent variables, such that the v-Net and g-Net are fully activated and optimized jointly with the P-Net. The P-Net takes the Fourier-mapped features $\{x, y, t\}$ as inputs and outputs the pressure field P , while the v-Net and g-Net take the spatial coordinates $\{x, y\}$ as inputs and output v and g , respectively. Notably, the predicted v and g fields are directly substituted into the governing partial differential equations (PDEs). Similar to the forward modeling case, the gradients of P with respect to the input coordinates are evaluated using automatic differentiation.

These differential terms are then substituted into the loss function constructed by concerned physical laws, including the govern-

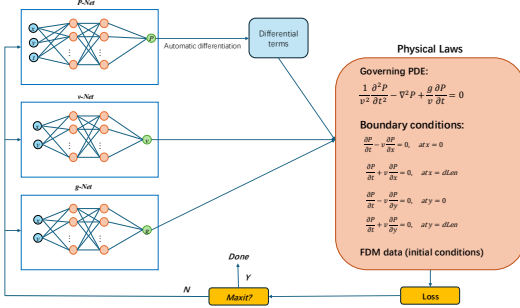


Figure 1. Overview of the proposed PINN framework for viscoacoustic wave propagation, including the network architecture and the constraint of physical laws. Three separate DNNs are used to approximate the pressure P , velocity v , and absorption coefficient g , respectively. Note that v -Net and g -Net are only activated in inversion mode. Automatic differentiation is exploited for obtaining the derivative terms and further constructing the loss function.

ing equations, boundary conditions, and initial conditions. The loss function can be summarized as:

$$\mathcal{L} = \lambda_p \mathcal{L}_{PDE} + \lambda_b \mathcal{L}_{BC} + \lambda_d \mathcal{L}_{Data} \quad (10)$$

Where \mathcal{L}_{BC} , \mathcal{L}_{PDE} , and \mathcal{L}_{Data} represent the mean squared error (MSE) of the boundary condition mismatch, the governing equation residuals, and the data misfit, respectively.

It is worth noting that while \mathcal{L}_{BC} remains identical, the definitions of \mathcal{L}_{PDE} and \mathcal{L}_{Data} differ slightly between the forward and inverse modes. Specifically, in the forward mode, the parameters v and g are fixed. In this case, \mathcal{L}_{PDE} minimizes the residuals of the governing equations to solve for the wavefield P in a known medium, while \mathcal{L}_{Data} serves as an initial constraint that enforces consistency with the initial state provided by the finite-difference method (FDM).

In the inverse mode, the parameters v and g are treated as learnable variables. Consequently, \mathcal{L}_{PDE} jointly optimizes the wavefield and the medium parameters, ensuring that the recovered v and g satisfy the governing physical laws. Meanwhile, \mathcal{L}_{Data} acts as an observation constraint derived from FDM simulations to drive the reconstruction of subsurface properties.

Here, λ_p , λ_b , and λ_d are weighting coefficients that balance the different loss terms and are treated as user-defined hyperparameters.

4 COMPUTATIONAL EXPERIMENTS

In this section, a series of computational experiments are implemented to validate the capability of the proposed PINN framework in solving forward and inverse problems for viscoacoustic wave propagation. We consider a 2D heterogeneous domain with a unified velocity or two-layered velocity model, while the viscoacoustic equation is solved within the domain. Furthermore, the inference stage is designed to evaluate the surrogate model's capability to capture the attenuation mechanism by both the variation of time-domain waveforms and frequency components. In addition, case 2 demonstrates the framework's ability to jointly solve for the forward wavefield and reconstruct the physical parameters.

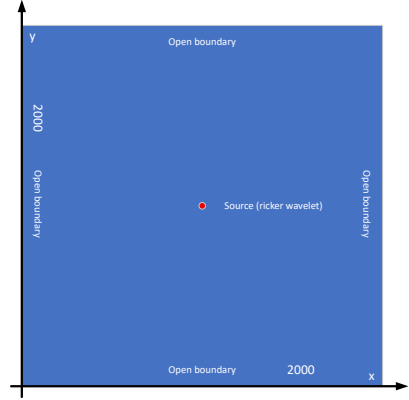


Figure 2. The spatial domain in case 1. Open boundary conditions are applied at four boundaries.

4.1 Domain Definition

We consider the same $2 \text{ km} \times 2 \text{ km}$ rectangular domain for all experiments. A Ricker wavelet source located at the center of the domain is employed as the seismic source, which can be analytically expressed as:

$$s(t) = (1 - 2(\pi f_0(t - t_0))^2) \exp(-(\pi f_0(t - t_0))^2) \quad (11)$$

where the dominant frequency is set to $f_0 = 5 \text{ Hz}$, and the peak time delay is set to $t_0 = 0.2 \text{ s}$. In addition, the total time duration is defined as 950 ms.

4.2 Case1: One-layer velocity model

In the first experiment, we consider a two-dimensional rectangular homogeneous domain with a uniform propagation velocity of 2 km/s . The computational domain is illustrated in Fig. 2. While the absorption coefficient is computed using Eq. (2), the quality factor Q is analytically derived from Li's empirical formula (3).

In this case, we sample 4,096 collocation points per batch within the interior domain to minimize the residuals of the viscoacoustic wave equation. Additionally, 1,024 points are sampled along the domain boundaries to impose the open boundary conditions, allowing seismic waves to propagate out of the truncated domain without artificial reflections. To avoid point-source singularities, wavefields at initial timesteps (150, 200, 250, and 300 ms) are used as initial constraints.

The network is trained using the Adam optimizer, and the selection of hyperparameters is detailed in the Appendix. Furthermore, the reference solutions and training datasets are generated using the finite-difference method (FDM). Specifically, we employ the open-source framework Devito (Louboutin et al. (2019)) to numerically solve the wave equation.

The comparative results are presented in Figs. 3–5. These figures demonstrate that the proposed PINN framework closely matches the ground truth. The performance of the PINN model is evaluated from three perspectives.

Firstly, we compare the wavefield snapshots predicted by PINNs and FDM. As shown in Fig. 3, the snapshots produced by PINNs are in good agreement with the FDM results. Moreover, at later timesteps (e.g., 950 ms), the PINN-predicted wavefields ex-

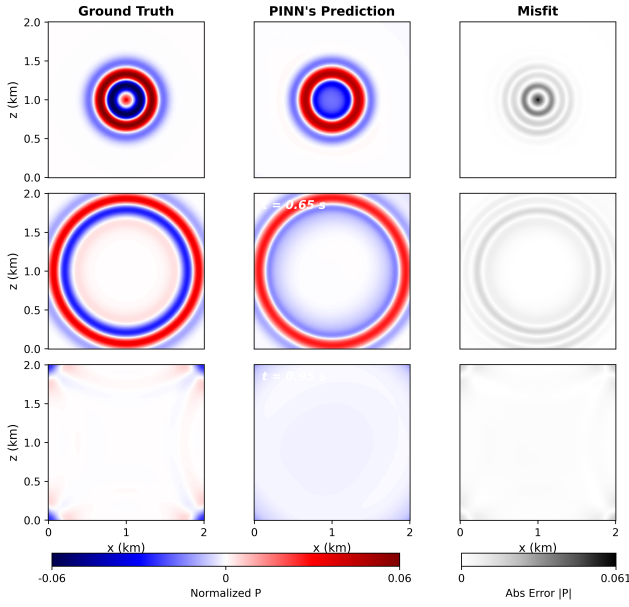


Figure 3. The results of pressure field distributions obtained from our proposed PINN and FDM in Case 1. We select three representative snapshots (i.e., $t = 0.35, 0.65, 0.95$ s) for comparison.

hibit significantly fewer boundary reflections compared to those obtained by the FDM method.

Secondly, amplitude variation is analyzed to assess whether the proposed framework correctly reproduces the physical attenuation behavior. Specifically, peak amplitude-distance curves extracted along the lower midline ($x = 1, y \in [0, 0.8]$) are compared between the PINN and FDM solutions, as shown in Fig. 4.

To further quantify the amplitude behavior, in a viscoacoustic medium, the attenuation of the peak amplitude A with respect to the propagation distance r can be expressed as

$$A(r, f) = A_0(f) \cdot \frac{1}{\sqrt{r}} \cdot e^{-\alpha(f)r} \quad (12)$$

where A_0 denotes the initial amplitude at the source, r is the propagation distance, and α is the frequency-dependent attenuation coefficient, defined as

$$\alpha(f) = \frac{\pi f}{vQ}, \quad (13)$$

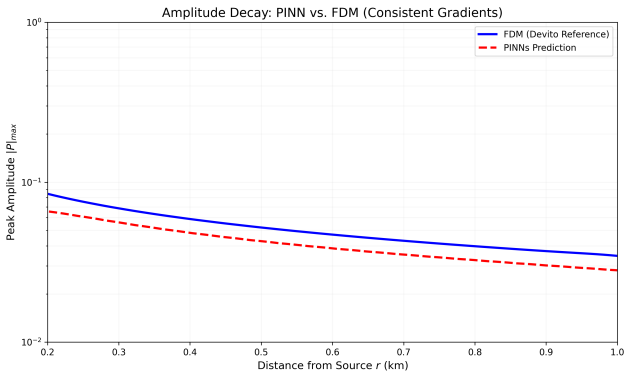


Figure 4. Comparison of amplitude decay rate for PINNs (red) and FDM (blue) in case 1

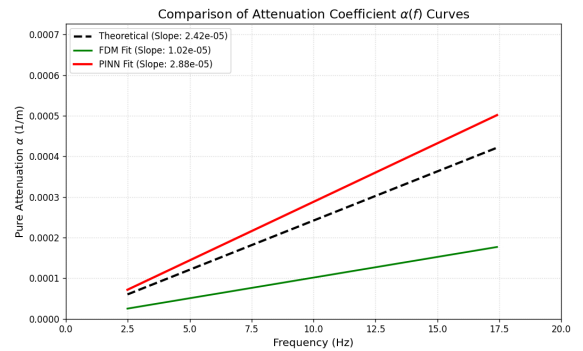


Figure 5. $\alpha-f$ curves by PINNs, FDM, and the analytical solution.

where f is the dominant frequency of the seismic wave, Q is the quality factor, and v is the propagation velocity. According to Li's empirical formula (3), the quality factor Q depends only on the velocity v . Since both v and Q are assumed to be spatially constant in this experiment, the theoretical attenuation coefficient $\alpha(f)$ exhibits a linear dependence on the frequency f . Consequently, the $\alpha-f$ relationships derived from the PINN and FDM simulations are compared against this theoretical linear trend to evaluate their respective abilities to capture intrinsic attenuation.

Figure 5 compares the attenuation coefficient $\alpha(f)$ estimated using different methods. The PINN-based results show significantly better agreement with the theoretical linear attenuation trend than those obtained using the finite-difference method (FDM). The theoretical attenuation slope is 2.42×10^{-5} , while the slope derived from the PINN results is 2.88×10^{-5} , corresponding to a relative error of 19.05%. In contrast, the FDM yields a slope of 1.02×10^{-5} , with a substantially larger relative error of 58.01%. Although both methods capture the overall frequency-dependent increase in attenuation, the PINN estimates exhibit a more consistent linear behavior across the 2–18 Hz frequency band. The larger deviation observed in the FDM results is attributed to numerical dissipation and dispersion inherent to grid-based schemes, whereas the physics-informed formulation enables PINNs to better preserve the underlying viscoacoustic attenuation law.

Furthermore, to evaluate the robustness of the proposed PINN framework with respect to discretization density in comparison with the traditional finite-difference method, a comparative sensitivity analysis is conducted. While FDM relies on discrete grid points to approximate partial derivatives, PINNs utilize randomly sampled collocation points to evaluate the residuals of the governing partial differential equations. To ensure a fair comparison, the “resolution” for both methods is defined in terms of the total number of sampling points used per time step within the computational domain.

Specifically, a series of parallel experiments is performed by progressively downsampling the resolution. For the FDM, the spatial grid spacing is gradually increased (i.e., the grid is coarsened). For the PINN framework, the batch size N of collocation points sampled within the domain is progressively reduced. The resulting wavefields and waveforms obtained using PINNs and FDM at different resolutions are then compared to assess the stability and robustness of the proposed PINN approach.

Figures 6 and 7 present a comparative analysis of the PINN and FDM results under different discretization resolutions. As shown in Fig. 6, as the grid spacing increases, the FDM solution

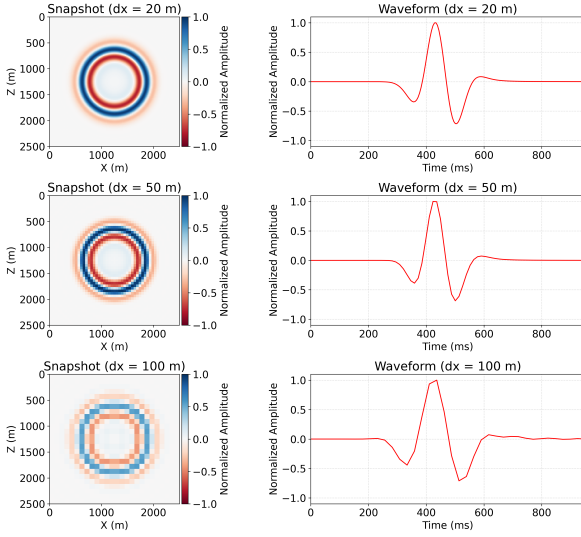


Figure 6. Wavefields and waveforms of FDM at different grid size

exhibits pronounced numerical dispersion, manifested by a loss of waveform fidelity and a breakdown of wavefront coherence. Specifically, when the grid spacing is increased to $\Delta x = 100.0$ m (coarse-grid scenario), the FDM solution suffers from severe structural distortion. The wavefront loses its coherent circular shape and becomes visibly pixelated. More critically, the waveform recorded at the monitoring point (right panel) reveals distinct spurious oscillations trailing the main wave packet. These high-frequency tail artifacts are non-physical and indicate that the numerical scheme fails to preserve waveform integrity under coarse discretization.

In contrast, Fig. 7 demonstrates that the wavefields and waveforms predicted by the PINN framework remain highly stable as the number of collocation points decreases. Even under the extremely

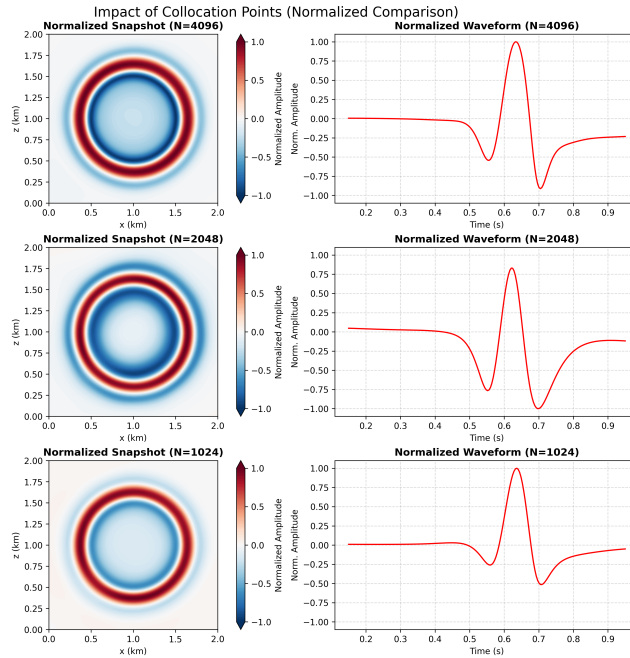


Figure 7. Wavefields and waveforms of PINNs at different collocation points

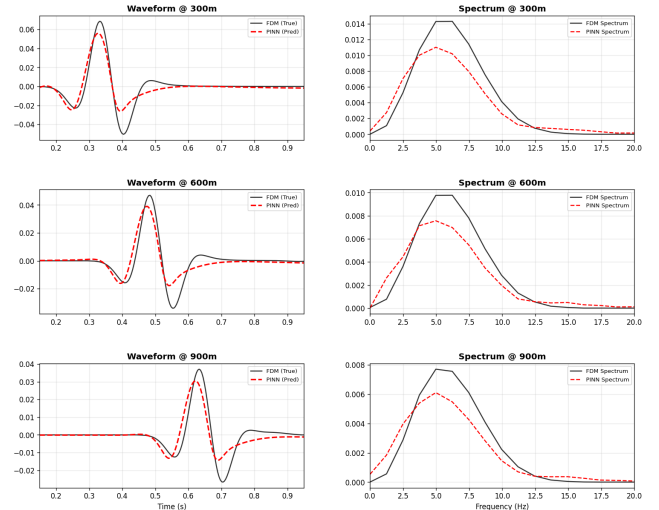


Figure 8. Waveform and frequency component comparison for PINNs (red) and FDM (black) in case 1

sparse sampling condition of only 1,024 collocation points, the PINN model maintains a smooth and coherent wavefield structure, effectively suppressing the spurious tail oscillations (i.e., numerical dispersion) that typically plague FDM solutions at comparable coarse resolutions.

Finally, to further validate the fidelity of the proposed PINN framework, comprehensive comparisons of time-domain waveforms and their corresponding frequency spectra are conducted at multiple propagation distances (300 m, 600 m, and 900 m), as shown in Fig. 8. While the frequency-domain analysis confirms that the dominant frequency is accurately preserved, the predicted waveforms (red dashed lines) exhibit a high degree of phase synchronicity and structural similarity with the FDM benchmarks (black solid lines). This agreement demonstrates the capability of the proposed PINN framework to accurately capture both the temporal evolution and phase velocity of the wavefield.

4.3 Two-layer velocity model

In the second experiment, we extend the application of the proposed framework to a heterogeneous medium in order to evaluate its robustness in more complex geological settings. In this scenario, both forward modeling and inverse analysis are integrated to demonstrate the capability of the unified framework to reconstruct velocity and attenuation fields from random initializations, thereby highlighting its potential for data-efficient seismic exploration.

As illustrated in Fig. 9, the computational domain consists of a two-layer velocity structure. The upper layer is characterized by a uniform propagation velocity of 1 km/s, while the lower layer maintains a velocity of 2 km/s. This configuration introduces a sharp impedance contrast at the horizontal interface, providing a rigorous test of the model's ability to enforce the viscoacoustic governing equations across spatially varying physical properties. Similarly, the absorption coefficient g is computed using Eq. (2), and the quality factor Q is analytically derived from Li's empirical formula (3).

Consistent with the first experiment, open boundary conditions are imposed on all four boundaries to suppress artificial reflections. In addition, wavefields at several initial timesteps are employed as constraints to circumvent the point-source singularity.

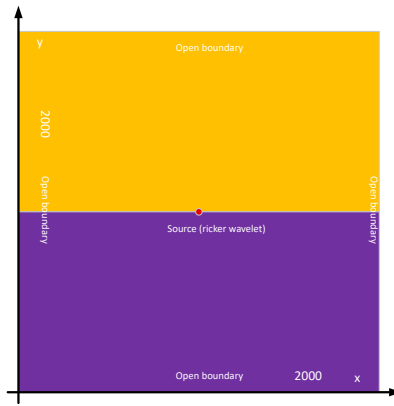


Figure 9. The spatial domain in case 2. Open boundary conditions are applied at four boundaries

The comparative results between the PINN predictions and the FDM reference solutions are presented in Figs. 10–12. The performance of the proposed framework in this heterogeneous scenario is evaluated using the following metrics.

First, similar to the first experiment, we compare the wavefield snapshots predicted by the PINN framework with those obtained from the FDM reference. As shown in Fig. 10, the PINN-predicted snapshots are in good agreement with the FDM results (ground truth), demonstrating the framework's capability to resolve distinct velocity regimes in a heterogeneous medium. Moreover, the snapshots reveal a distinctive characteristic of the PINN-based solver. Unlike the traditional FDM solution, which exhibits a numerically “closed” wavefront due to grid-based coupling across the material interface, the PINN prediction clearly captures the physical decoupling at the layer boundary. This behavior indicates that PINNs exhibit higher sensitivity to sharp impedance contrasts, accurately recovering the independent propagation characteristics of each layer without introducing artificial numerical smoothing.

Figures 11 and 12 present (a) the ground-truth models, (b) the initial guess models used by the PINN framework, and (c) the corresponding inversion results for the velocity and absorption coefficient fields. These results demonstrate that the proposed PINN framework is capable of successfully recovering both the velocity and absorption distributions from observed data, even when starting from random initial models.

It is important to distinguish between the procedure used to generate the ground-truth models and the inversion strategy adopted by the PINN framework. Although the synthetic absorption coefficient g is generated from the velocity v using Li's empirical $Q-v$ relationship, this physical coupling is not imposed in either the network architecture or the loss function. During training, the velocity and absorption fields are initialized randomly and inverted as two independent parameters. Consequently, the accurate reconstruction of both fields indicates that the PINN framework is capable of disentangling kinematic effects (associated with v) and attenuation effects (associated with g) directly from the seismic wavefield, without relying on hard-coded rock-physics constraints.

The successful inversion demonstrates that PINNs can infer the correct physical parameters, including the correct interface and gradient changes, by minimizing the loss function under conditions of time sparsity and random initialization, suggesting that the pro-

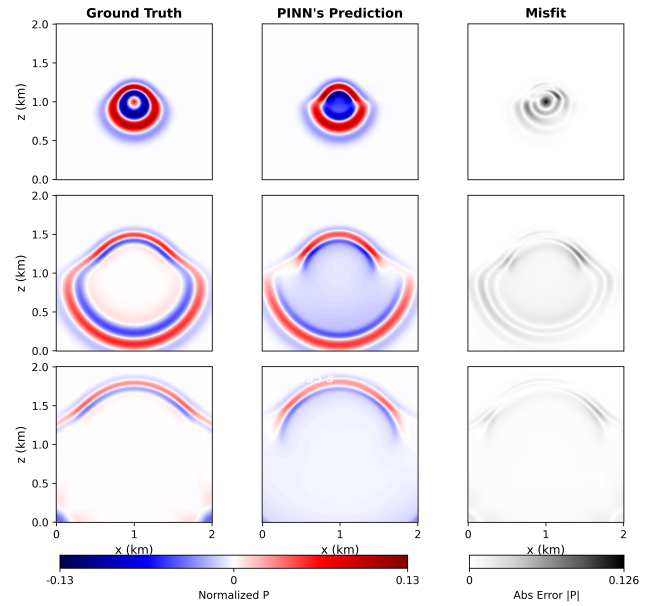


Figure 10. The results of pressure field distributions obtained from our proposed PINN and FDM in Case 2. We select three representative snapshots (i.e., $t = 0.35, 0.65, 0.95$ s) for comparison.

posed PINN approach offers a promising, data-efficient alternative to conventional inversion methods.

5 DISCUSSIONS

This study adopts a viscoacoustic governing equation derived from (Deng & McMechan(2007)) as a pragmatic numerical approximation of viscoacoustic wave propagation. By introducing a first-order temporal derivative as an effective damping term, the original hyperbolic wave equation is transformed into a weakly parabolic form to emulate intrinsic attenuation effects. This formulation assumes frequency-independent velocity and quality factor within a limited bandwidth and therefore does not strictly satisfy causality, which in true viscoacoustic media requires velocity dispersion. In the proposed framework, a fixed reference frequency corresponding to the dominant source frequency is used to compute the absorption coefficient. Although this approximation neglects subtle frequency-dependent dispersion effects, it successfully captures the macroscopic amplitude decay and geometric spreading compensation required for seismic imaging and inversion at exploration scales. More importantly, this formulation yields a numerically stable and differentiable residual, which is particularly advantageous for training physics-informed neural networks.

A critical finding of this study is the fundamentally different failure behaviors exhibited by the finite-difference method (FDM) and PINNs under low-resolution conditions. Sensitivity analyses indicate that FDM suffers from a threshold-type failure: once the grid spacing exceeds the numerical stability limit (e.g., $\Delta x = 100$ m), severe numerical dispersion emerges, characterized by spurious oscillatory tails and pronounced phase distortion. In contrast, the proposed PINN framework demonstrates a graceful degradation behavior. Even under extremely sparse sampling conditions, such as using only 1,024 collocation points, the solution remains stable, albeit with reduced accuracy. This robustness primarily arises from the fundamentally different solution paradigms

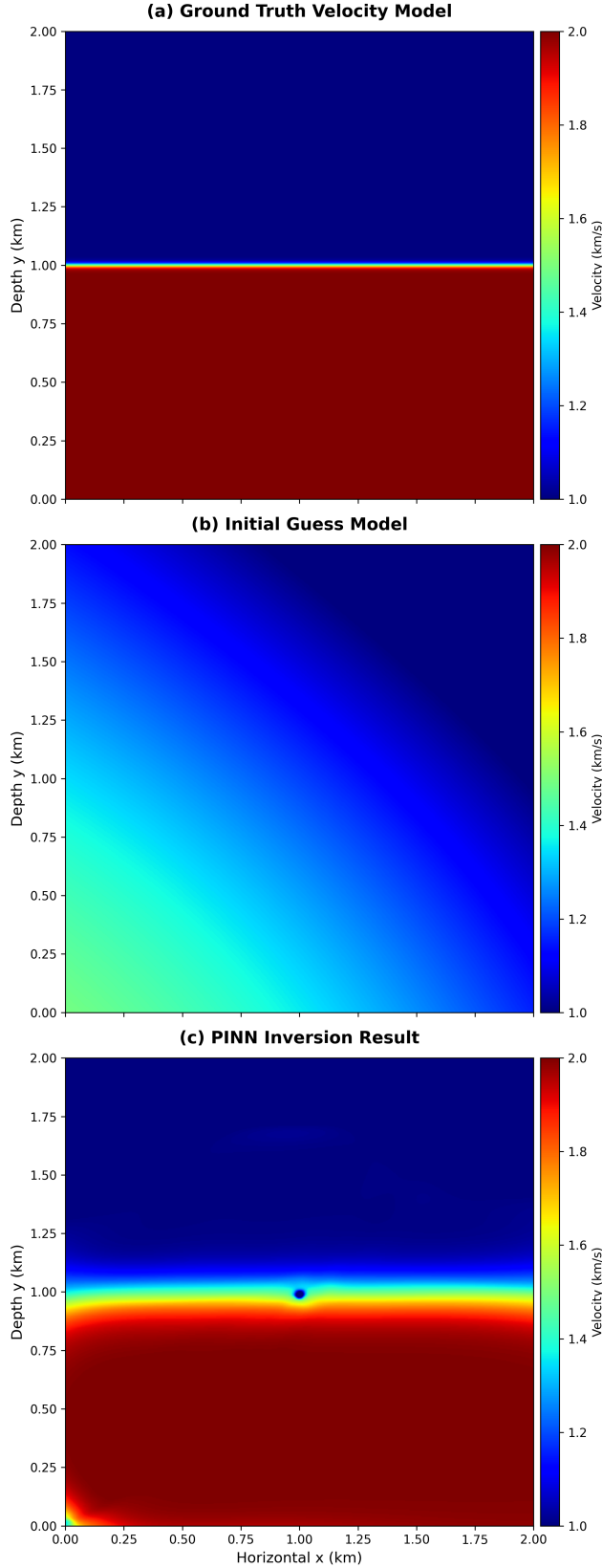


Figure 11. Ground truth, initial model, and PINN-based inversion result for velocity v

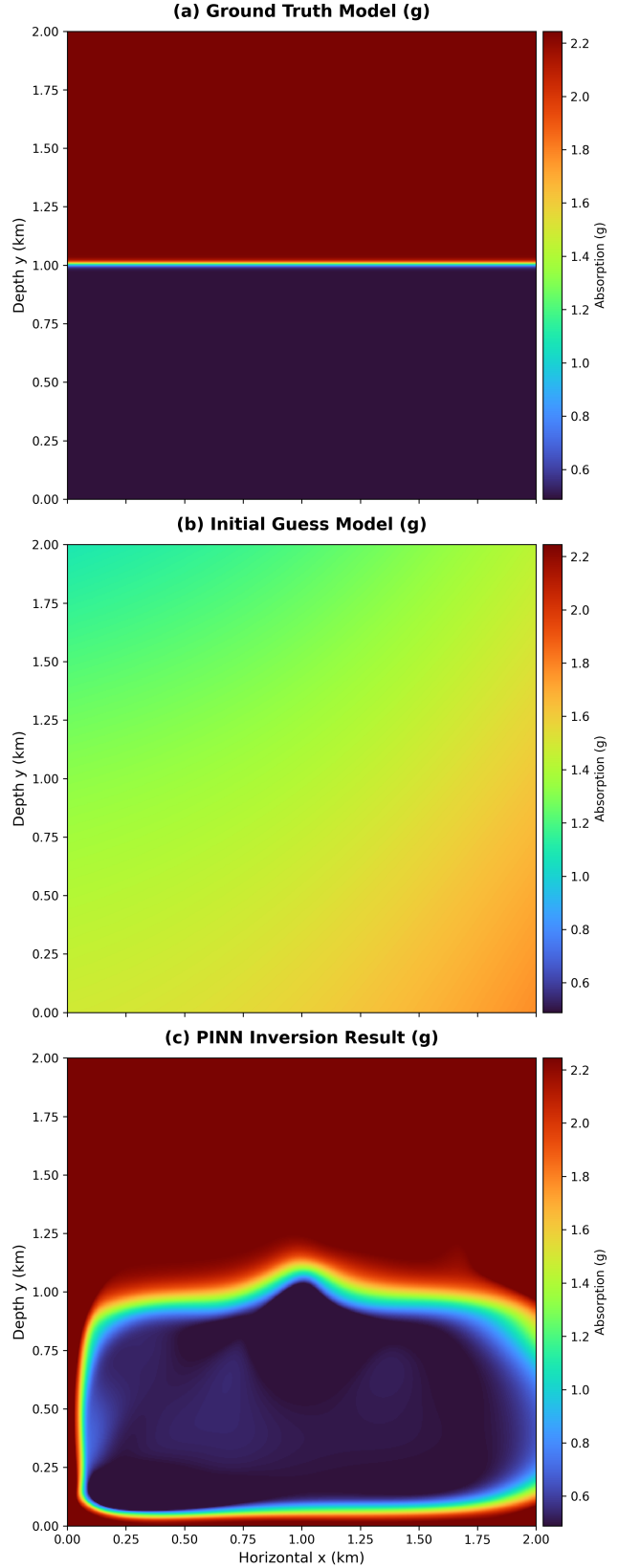


Figure 12. Ground truth, initial model, and PINN-based inversion result for absorption coefficient g

of PINNs and FDM. While FDM relies on local, grid-based time marching and is therefore highly sensitive to discretization thresholds, PINNs formulate wave propagation as a global optimization problem constrained by the governing equations. Stochastic resampling of collocation points further enhances this property by improving coverage of the spatiotemporal domain during training.

The successful recovery of both velocity and attenuation fields from stochastic initial models further demonstrates that PINNs can effectively solve inverse problems by treating physical parameters as learnable variables. Unlike traditional forward modeling approaches with fixed model parameters, the PINN framework simultaneously optimizes the neural network weights and physical parameters (velocity and attenuation) through gradient-based optimization, thereby enabling unified forward and inverse modeling within a single framework.

Nevertheless, several limitations of the PINN framework should be acknowledged. First, the spectral bias inherent to deep neural networks leads to preferential learning of low-frequency components, resulting in diminished high-frequency content compared to FDM solutions. Second, for simple forward modeling tasks, PINNs are computationally less efficient than classical FDM solvers, as iterative optimization is required even for homogeneous models. Finally, the performance of PINNs remains sensitive to hyperparameter selection, particularly the weighting of different loss components.

Future work will focus on adaptive loss-weighting strategies and automated hyperparameter optimization to improve robustness across different physical regimes. In addition, advanced network architectures incorporating attention mechanisms, such as Transformer-based models, may help mitigate spectral bias and better capture long-range dependencies in seismic wavefields.

6 CONCLUSION

This study presents a physics-informed neural network (PINN) framework for viscoacoustic wave modeling and inversion. By incorporating an effective damping formulation to approximate intrinsic attenuation, the proposed approach enables a stable representation of viscoacoustic wave propagation. Numerical experiments demonstrate that both velocity and absorption fields can be successfully recovered from random initial models, highlighting the inversion capability of PINNs by treating physical parameters as learnable variables. Another key observation is the fundamentally different behavior exhibited by PINNs and finite-difference methods under coarse discretization or data-scarce conditions. While finite-difference solvers suffer from abrupt failure due to numerical dispersion once stability limits are exceeded, the PINN framework exhibits a gradual degradation in accuracy while maintaining solution stability. These results suggest that PINNs provide a flexible and robust alternative for viscoacoustic seismic modeling and inversion, particularly in scenarios where dense spatial or temporal sampling is impractical.

ACKNOWLEDGEMENTS

Liang CH gratefully acknowledges the continuous guidance and support of his supervisor, Professor Jun Matsushima, as well as the revisions and geophysical insights provided by Dr. Peng XL. He also sincerely thanks the co-supervisor, Professor Katsumori Mizuno, for his specialized and insightful suggestions. In

addition, special thanks are extended to former visiting PhD student Lou JS and all colleagues in the laboratory for their constructive discussions related to this thesis.

REFERENCES

Alfarraj, M. & AlRegib, G., 2019. Semi-supervised learning for acoustic impedance inversion, in *SEG Technical Program Expanded Abstracts*, pp. 2298–2302, doi: 10.1190/segam2019-3215902.1.

Alkhalifah, T., Song, C., Waheed, U. B., & Hao, Q., 2021. Wavefield solutions from machine learned functions constrained by the helmholtz equation, *Artificial Intelligence in Geosciences*, **2**, 11–19, doi: 10.1016/j.aiig.2021.08.002.

Deng, F. & McMechan, G. A., 2007. True-amplitude prestack depth migration, *Geophysics*, **72**(3), S155–S166, doi: 10.1190/1.2714334.

Haghigat, E., Raissi, M., Moure, A., Gomez, H., & Juanes, R., 2021. A physics-informed deep learning framework for inversion and surrogate modeling in solid mechanics, *Computer Methods in Applied Mechanics and Engineering*, **379**, 113741, doi: 10.1016/j.cma.2021.113741.

Li, C., Liu, X., & Zu, S., 2025. Seismic data reconstruction via least-squares generative adversarial networks with inverse interpolation, *IEEE Transactions on Geoscience and Remote Sensing*, **63**, 1–16, doi: 10.1109/TGRS.2025.3540453.

Liu, Y. & Sen, M. K., 2011. Scalar wave equation modeling with time-space domain dispersion-relation-based staggered-grid finite-difference schemes, *Bulletin of the Seismological Society of America*, **101**(1), 141–159.

Louboutin, M. et al., 2019. Devito (v3.1.0): an embedded domain-specific language for finite differences and geophysical exploration, *Geoscientific Model Development*, **12**(3), 1165–1187, doi: 10.5194/gmd-12-1165-2019.

Malinowski, M., Operto, S., & Ribodetti, A., 2011. High-resolution seismic attenuation imaging from wide-aperture onshore data by visco-acoustic frequency-domain full-waveform inversion, *Geophysical Journal International*, **186**(3), 1179–1204, doi: 10.1111/j.1365-246X.2011.05098.x.

Nogueira, P. & Porsani, M. J., 2021. 3d reverse time migration using a wavefield domain dynamic approach, *Journal of Applied Geophysics*, **190**, 104345, doi: 10.1016/j.jappgeo.2021.104345.

Pled, F. & Descliers, C., 2022. Review and recent developments on the perfectly matched layer (pml) method for the numerical modeling and simulation of elastic wave propagation in unbounded domains, *Archives of Computational Methods in Engineering*, **29**(1), 471–518, doi: 10.1007/s11831-021-09581-y.

Raissi, M., Perdikaris, P., & Karniadakis, G. E., 2019. Physics-informed neural networks: A deep learning framework for solving forward and inverse problems involving nonlinear partial differential equations, *Journal of Computational Physics*, **378**, 686–707, doi: 10.1016/j.jcp.2018.10.045.

Raissi, M., Yazdani, A., & Karniadakis, G. E., 2020. Hidden fluid mechanics: Learning velocity and pressure fields from flow visualizations, *Science*, **367**(6481), 1026–1030, doi: 10.1126/science.aaw4741.

Rasht-Behesht, M., Huber, C., Shukla, K., & Karniadakis, G. E., 2021. Physics-informed neural networks (pinns) for wave propagation and full waveform inversions, *arXiv preprint arXiv:2108.12035*, doi: 10.48550/arXiv.2108.12035.

Ren, P., Rao, C., Chen, S., Wang, J.-X., Sun, H., & Liu, Y., 2022. Seismicnet: Physics-informed neural networks for seismic wave modeling in semi-infinite domain, *arXiv preprint arXiv:2210.14044*.

Virieux, J. & Operto, S., 2009. An overview of full-waveform inversion in exploration geophysics, *Geophysics*, **74**(6), WCC1–WCC26, doi: 10.1190/1.3238367.

Wong, H. S., Chan, W. X., Mao, W., & Yap, C. H., 2025. 3d velocity and pressure field reconstruction in the cardiac left ventricle via physics informed neural network from echocardiography guided by 3d color doppler, *Computer Methods and Programs in Biomedicine*, **263**, 108671, doi: 10.1016/j.cmpb.2025.108671.

Wu, Y. & Lin, Y., 2020. Inversionnet: An efficient and accurate data-driven full waveform inversion, *IEEE Transactions on Computational Imaging*, **6**, 419–433, doi: 10.1109/TCI.2019.2956866.

Zhao, Z., Wang, Y., Zhang, W., Ba, Z., & Sun, L., 2025. Physics-informed neural networks in heat transfer-dominated multiphysics systems: A comprehensive review, *Engineering Applications of Artificial Intelligence*, **157**, 111098, doi: 10.1016/j.engappai.2025.111098.

Zou, J., Liu, C., Zhao, P., & Song, C., 2024. Seismic wavefields modeling with variable horizontally layered velocity models via velocity-encoded pinn, *IEEE Transactions on Geoscience and Remote Sensing*, **62**, 1–11, doi: 10.1109/TGRS.2024.3411472.